ACS Photonics

Article

Cite This: ACS Photonics 2019, 6, 2570−2576

pubs.acs.org/journal/apchd5

# Correlative Dark-Field and Photoluminescence Spectroscopy of Individual Plasmon−Molecule Hybrid Nanostructures in a Strong Coupling Regime

Martin Wersäll,[†] Battulga Munkhbat,[†] Denis G. Baranov,[†] Felipe Herrera,[‡] Jianshu Cao,[§] Tomasz J. Antosiewicz,[†,∥] and Timur Shegai*[,†]

[†]Department of Physics, Chalmers University of Technology, 412 96, Göteborg, Sweden

[‡]Department of Physics, Universidad de Santiago de Chile, Avenida Ecuador 3943, Santiago, Chile

[§]Department of Chemistry, Massachusetts Institute of Technology, 77 Massachusetts Avenue, Cambridge, Massachusetts 02139, United States

[∥]Faculty of Physics, University of Warsaw, Pasteura 5, 02-093 Warsaw, Poland

Supporting Information

**ABSTRACT:** Light−matter interactions play a crucial role in several prominent nano-optical phenomena, such as plasmon-mediated fluorescence, nanoscale lasing, and strong plasmon−exciton coupling. The latter holds promise for the development of nanoscale nonlinear optical schemes and room-temperature polaritonic lasers. In recent years, strong coupling in nanoscale plasmon−exciton systems, also known as plasmon−exciton polaritons, has been thoroughly investigated using transmission, reflection, and dark-field scattering spectroscopies. However, only a few recent studies performed experiments using photoluminescence spectroscopy on the individual hybrid nanostructure level. The latter is important for the detailed understanding of intrinsic excited state dynamics in strongly coupled systems. Here, we use correlative dark-field scattering (DF) and photoluminescence (PL) measurements to study polaritonic states in individual silver nanoprisms surrounded by molecular *J*-aggregates. We investigate these systems under various experimental conditions, including temperatures in the range $T = 4-300$ K, laser excitation wavelengths at 532, 568, and 640 nm, and a broad range of plasmon−exciton detunings. Our findings indicate that the lower energy peak in PL emission closely follows the lower polariton band observed in DF, while the higher energy PL peak follows the emission of uncoupled *J*-aggregate molecules and incoherent states. These observations further improve the understanding of excited state dynamics in strongly coupled plasmon−exciton systems.

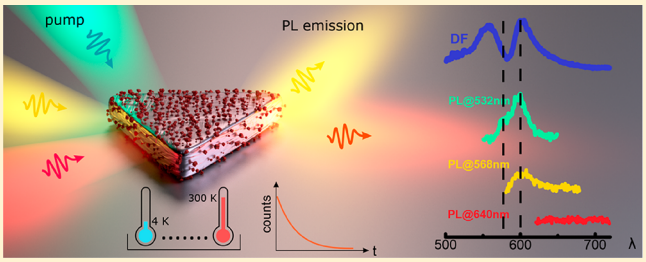


**KEYWORDS:** *strong coupling, surface plasmon, plasmon−exciton coupling, photoluminescence, single nanoparticle spectroscopy, J-aggregates*



Strong coupling between collective electronic excitations, plasmons, in noble metal nanoparticles and optical absorption bands in organic chromophores have attracted significant research interest recently.[1,2] In this regime, the rate of coherent energy exchange between the plasmonic and molecular subparts exceeds their respective dissipation rates. To achieve sufficient coupling strength, a single plasmonic nanoparticle is often coupled to many chromophores, thereby forming coherent polaritonic states and a multitude of dark incoherent states. In the first approximation, such a situation can be modeled by a single cavity mode coupled to $N \gg 1$ noninteracting emitters. This is known as the Tavis−Cummings model.[3] The diagonalization of the Tavis−Cummings Hamiltonian results in two coherent bright polaritonic states, upper and lower polaritons, and $N - 1$ dark polaritonic states, whose photonic component is negligible. The existence of these bright and dark states, as well as the interplay between them, is crucial for relaxation processes in such hybrid systems.[4−8]

Following these concepts, many recent experiments have demonstrated strong coupling using high concentrations of organic dyes interacting with various optical resonators, such as propagating surface plasmons in thin metal films, Fabry−Pérot microcavities, and plasmonic nanoparticle arrays.[9−15] More recently, experimental studies on single nanoparticle systems coupled to molecular excitons,[16−19] as well as excitons in transition metal dichalcogenides,[20−24] have been reported. Furthermore, several recent works claimed achieving strong coupling using individual quantum emitters, such as colloidal quantum dots[25−27] and organic dyes.[28]

**Received:** July 26, 2019
**Published:** September 9, 2019




DOI: 10.1021/acsphotonics.9b01079
ACS Photonics 2019, 6, 2570−2576

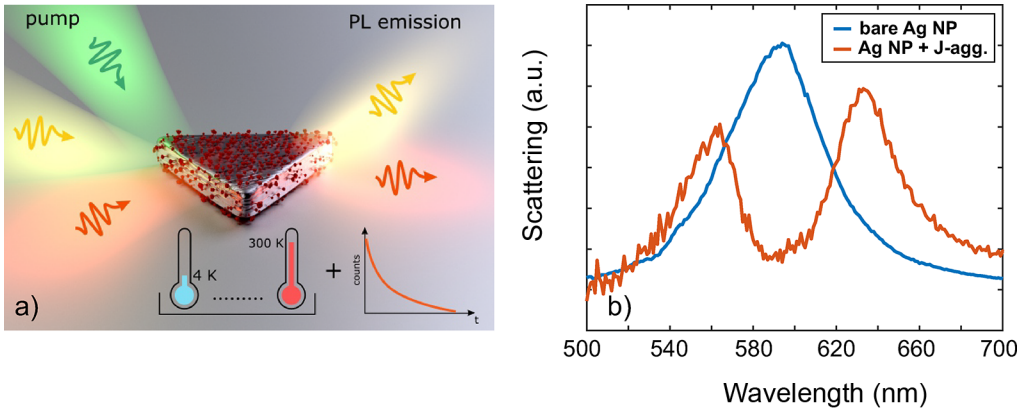


**Figure 1.** (a) Sketch of a nanoscale plasmon-exciton hybrid system—a single crystalline Ag nanoprism coated with *J*-aggregates of TDBC dye molecules, studied using PL and DF spectroscopy at different excitation lasers, temperatures ($T$ = 4–300 K), and plasmon–exciton detunings. (b) Comparison between a typical experimental DF scattering of an individual bare nanoprism (blue) and a nanoprism covered with *J*-aggregates (red). In the latter case, a clear mode splitting of ~250 meV is observed.

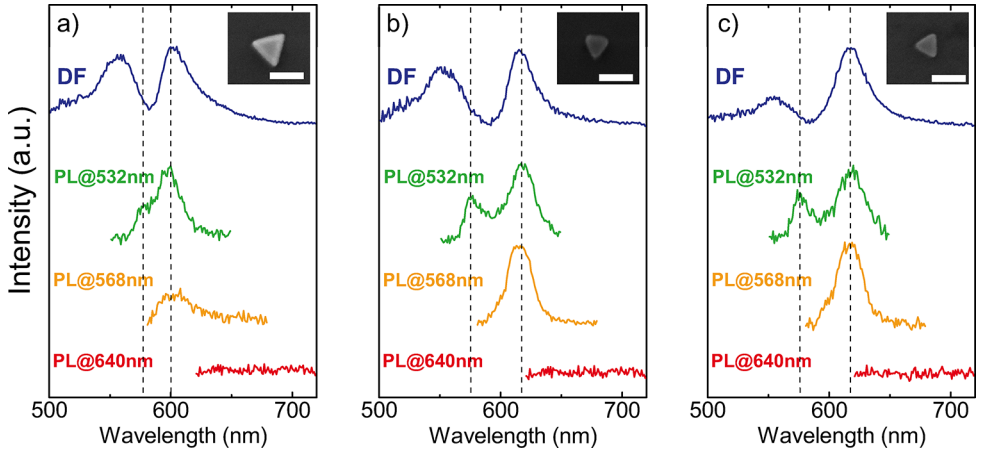


**Figure 2.** DF scattering (blue) and PL spectra of three different hybrid nanostructures excited by 532 (green), 568 (orange), and 640 nm (red) laser excitations. The particles in (a)–(c) are sorted left to right according to increasing vacuum Rabi splitting. The insets display SEM images of each corresponding hybrid nanostructure. The scale bars are 100 nm. All measurements were conducted at $T$ = 77 K in an optical cryostat. Vertical dashed lines are guides for an eye.

Most plasmon-molecule studies listed above have relied on elastic spectroscopies, such as DF scattering, to quantify strong coupling. However, inelastic PL spectra must also be affected by strong coupling, as has been theoretically predicted earlier.[7,29,30] Recently, several works have reported mode hybridization in PL signal from hybrid nanostructures, both on the ensemble and single nanoparticle level.[8,26,27,31] Detailed correlative studies are, however, relatively sparse.

Here, we perform a correlative dark-field and photoluminescence spectroscopy study using three different excitation wavelengths, 532, 568, and 640 nm, at different temperatures ($T$ = 4–300 K) and for various plasmon–exciton detunings. The temperature-dependent data reveal unusual spectroscopic behavior of polaritonic states, which allows assigning the lower energy PL emission peak to the lower polariton, whereas the higher energy emission peak is assigned to uncoupled molecules and incoherent states. Noteworthy, no PL emission at the upper polariton frequency was observed in this study even at $T$ = 4 K.

## RESULTS AND DISCUSSION

**System under Study.** Figure 1a shows the sketch of a hybrid nanostructure. We use thin (~10 nm) single-crystalline silver nanoprisms surrounded by *J*-aggregated TDBC molecules. The silver nanoprisms are about ~70 nm in side length, such that the localized surface plasmon resonance matches the *J*-aggregate absorption line (~588 nm). These hybrid nanostructures were synthesized in an aqueous solution using a photoinduced growth method (see Methods).

Our hybrid nanostructures exhibit Rabi splitting in DF on the order of ~200–250 meV, which exceeds both plasmon (~150–200 meV) and exciton (~50 meV) line widths (see Figure 1b). The single-crystalline nature and small dimensions of the silver nanoprisms result in relatively high quality factors for plasmonic nanoparticles $Q \sim 10–15$, as well as subwavelength effective mode volumes, which makes them optimal for strong coupling. Most hybrid nanostructures in this study fulfill the criterion for the strong coupling regime, in agreement with our previous studies.[8,19,32]

**PL with Varying Laser Excitation Wavelengths.** PL spectra from three different single nanoparticles, each of which were excited using three different laser excitations (532, 568, and 640 nm), together with the corresponding DF and scanning electron microscopy (SEM) images are shown in Figure 2. These measurements were conducted at $T$ = 77 K using an optical cryostat (see Methods). The nanoparticles are


DOI: 10.1021/acsphotonics.9b01079
ACS Photonics 2019, 6, 2570–2576

sorted left to right according to the increasing Rabi splitting to illustrate the PL and DF spectra differences between systems with varying coupling strengths. We additionally point out that under 532 nm excitation the PL spectra contain two resolved peaks, which we attribute to emission from incoherent dark states and uncoupled molecules (higher energy peak) and emission from the lower polariton (LP) state (lower energy peak). The arguments for this assignment will be provided further in the discussion.

The long-pass filters, which we employ to collect PL spectra for 568 and 640 nm laser excitations, allow transmitting wavelengths only above 580−590 nm. It is in this spectral range where the emission from uncoupled molecules or incoherent states occurs. Hence, the high energy peaks would be absent in the PL spectra, even if the PL pathways would actually allow this kind of emission process to occur. Thus, upon 568 nm excitation, we can only detect the lower polariton emission in PL. At 640 nm excitation, however, almost no PL signal was detected for any of the studied nanoparticles. This could be due to low probability of populating long-lived incoherent dark states under our experimental conditions. In particular, the Rabi splitting in our systems is quite high, around 200−250 meV, while the inhomogeneous width of *J*-aggregates is much narrower, which makes it unlikely to populate the long-lived states upon resonant excitation of LP state. To further explain these observations, we refer the reader to the Supporting Information (Appendix: the model and comparison to experiment) for the detailed discussion about the mechanism of PL from strongly coupled systems.

Note that the lower energy PL emission peaks are almost spectrally overlapped with the corresponding lower polariton peaks in DF, which implies that the lower energy PL peaks correspond to the lower polariton emission. This observation is in line with previous experimental results,[8] as well as with theoretical models of plasmon−exciton hybrid nanostructures in the strong coupling regime.[7,29,30]

Furthermore, in Figure 3 we show a correlation between all nanostructures that we measured in this study, sorted according to the increasing energy of the LP peak in DF. These experiments were conducted at $T$ = 77 K. The data contains higher energy and lower energy peaks extracted from DF spectra, as well as the corresponding peaks extracted from PL data obtained using 532 and 568 nm excitation (at 640 nm excitation, no emission was detected). For 532 nm excitation, we provide both the higher energy and lower energy PL peaks data.

We notice several important details upon closer inspection of Figure 3. First, the upper polariton (UP) peak in DF fluctuates somewhat for different nanoparticles (see blue squares in Figure 3). This is likely due to variation in Rabi splitting of different nanostructures, which arises due to variation in their geometrical parameters, as well as the number and possibly orientation of *J*-aggregates around those structures. Despite these significant fluctuations in UP DF data, however, the higher energy PL peak (see orange circles in Figure 3) shows nearly no fluctuations and correspondingly *no* correlation with the UP peak in DF. This observation, together with the fact that high energy PL peak is significantly to the red from the UP DF, allows ruling out the upper polaritonic origin of the higher energy PL peak.

Second, the LP in DF and lower energy PL peaks at both 532 and 568 nm laser excitations practically overlap with each other, which points to the lower polariton origin of the PL emission in this case, in agreement with data shown in Figure 2. The only deviation from this behavior is observed for particles with relatively low energy LPs (below 2.0 eVs). This could possibly be due to phonon-assisted relaxation pathway of PL in strongly coupled systems.[4−6,8] For strongly red-detuned particles, such relaxation requires large energy phonons. Those in turn might not be available to the system, as the phonon spectrum of *J*-aggregates has a high energy cutoff at around 1615 $cm^{-1}$, which corresponds to ∼200 meV (the high-frequency C−H vibrations occur at much higher frequencies of around 3500 $cm^{-1}$).[17,33] This suggests that LP energies in DF and PL may start deviating from each other for nanoparticles with energy gap between the incoherent states (at around 2.15 eV) and LP exceeding the high energy cutoff in the *J*-aggregate phonon spectrum ∼200 meV, that is, for LP DF energies below 1.95 eV. This agrees well with observations in Figure 3, thus, supporting the validity of phonon-assisted relaxation in this case.

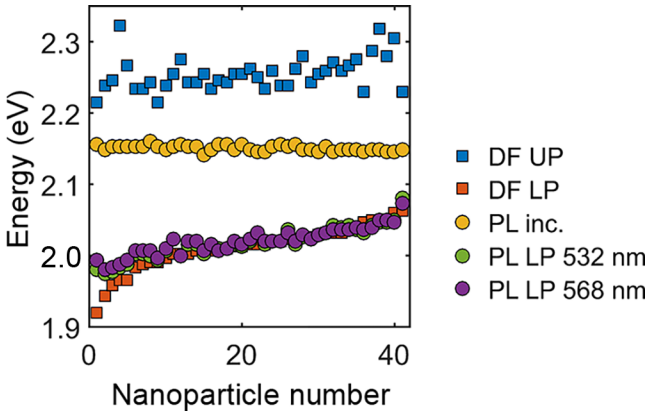


**Figure 3.** Correlative DF and PL (collected using 532 and 568 nm laser excitations) spectroscopy data, presented in terms of corresponding peak positions versus the nanoparticle number. The nanoparticles are arranged according to the increasing LP energy observed in DF. It is important to note that DF UP (blue squares) signal fluctuates, whereas higher energy PL peaks (orange circles) do not fluctuate with the nanoparticle number. This observation rules out the upper polariton origin of the higher energy PL peaks. At the same time the lower polariton DF and PL data at both excitation wavelengths are almost overlapping, confirming the polaritonic origin of lower energy PL peaks. All measurements were conducted at $T$ = 77 K in an optical cryostat.

**Role of Plasmon−Exciton Detuning.** Plasmon−exciton detuning plays an important role in the strong coupling, as it determines the composition of hybrid states. We will now study how PL depends on detuning between plasmon and exciton resonances in a hybrid system, $\delta = \omega_{pl} - \omega_0$. Since the energy difference between the dark incoherent states (also called exciton reservoir) and upper/lower coherent polaritonic states is equidistant only in the case of zero detuning, it is important to study how the relaxation processes alter when this condition is not met. For a strongly blue-detuned situation, the dark states are closer to the lower polariton state, whereas in the strongly red-detuned case the dark states are closer to the upper polariton. The plasmon−exciton detuning thus plays an important role in the relaxation pathways of a hybrid system, especially in light of the phonon-assisted relaxation processes described in the previous section (also see SI Appendix: the model and comparison to experiment). Indeed, plasmon-


DOI: 10.1021/acsphotonics.9b01079
ACS Photonics 2019, 6, 2570−2576

exciton detuning has been previously shown to substantially affect the photo-oxidation rate of *J*-aggregates in the strong coupling regime.[32] Similar observations were also recently made in more extended organic microcavities.[34]

In Figure 4, experimental DF together with PL from highly blue-detuned (a, b), as well as highly red-detuned (c, d),

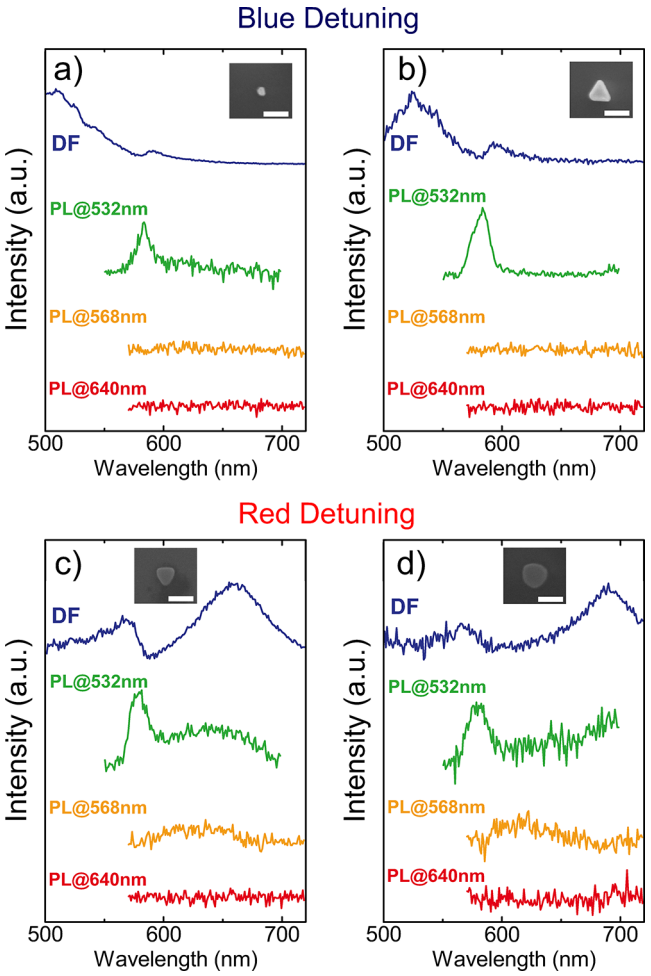


**Figure 4.** (a, b) Highly blue-detuned DF spectra, together with the corresponding PL spectra obtained using 532, 568, and 640 nm laser excitations. (c, d) Highly red-detuned DF spectra, together with the corresponding PL spectra obtained using 532, 568, and 640 nm laser excitations. Insets show corresponding SEM images. Scale bars are 100 nm. All measurements were conducted at $T$ = 77 K.

plasmon−exciton hybrid systems are shown. The key observations for blue-detuned nanoparticles are as follows. First, at 532 nm excitation, the emission from incoherent states is seen; however, at both 568 and 640 nm excitations, no detectable PL emission is observed. This is likely because the long-pass filters used for 568 and 640 nm excitations do not allow the incoherent molecular emission through. Moreover, the LP emission in this case is too close to the exciton reservoir, and thus cannot be efficiently populated by the phonon-assisted process.

For red-detuned particles, both incoherent states and LP emission are observed, similar to the close-to-zero detuning data in Figure 2. The only notable difference with respect to the latter is that the LP emission is relatively broad and shifted to the blue of the respective DF peak (in agreement with the low energy LP nanoparticles in Figure 3). These observations are in line with the Agranovich and Litinskaya formalism,[4−6] which is described in more details in the Appendix (see Supporting Information). In brief, this analytical formalism is based on the energy-conserving Fermi's golden rule and treats the polariton emission as a composition of phonon-assisted relaxation and radiative processes.

Finally, we note that, in addition to the static PL spectra at $T$ = 77 K, shown in Figures 2−4, we also performed lifetime measurements of the strongly coupled plasmon−molecule hybrids and compared them to bare *J*-aggregates. Unfortunately, the time resolution of our time correlated single-photon counting modules (TCSPC) did not allow to resolve the ultrafast dynamics in the *J*-aggregates beyond the instrument response function (IRF). These results are therefore inconclusive; nevertheless, we report them in the Supporting Information for the convenience of the readers (see SI, Figure S3).

**Temperature Dependence of Hybrid States Spectroscopy.** To further understand the relaxation processes of the hybrid structures in this study, we aim to investigate how both DF and PL spectra alter upon changes from cryogenic to room temperature. The main reason for this is that inelastic relaxations within hybrid systems involve phonon-assisted energy dissipation,[4−7,29,30,35−37] and exciton−phonon interactions are known to depend on temperature.[38] It is therefore natural to investigate the presence of any temperature effects.

The spectral changes when the temperature is raised from $T$ = 4−300 K, both in DF and PL, are shown in Figure 5. Note

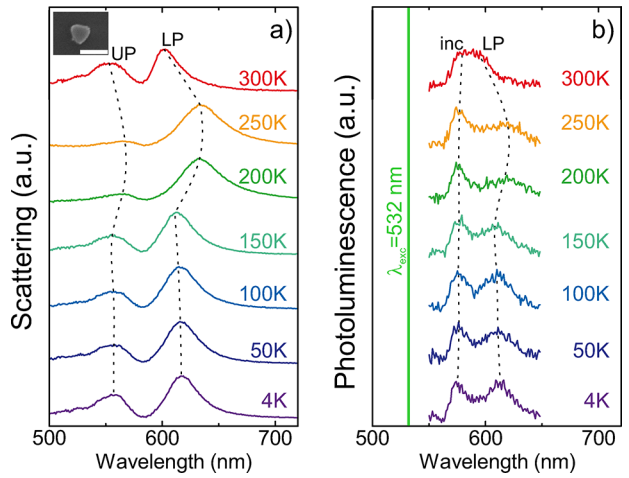


**Figure 5.** (a) Temperature-dependent DF spectra of a single hybrid nanostructure measured at $T$ = 4−300 K. The inset shows an SEM image of the corresponding nanoparticle. Scale bar is 100 nm. (b) PL spectra recorded under 532 nm laser excitation for the same hybrid nanostructure and at the same temperatures as in (a). Dashed lines are guides for the eye. Note the substantial red shift of both UP and LP peaks in DF observed at $T$ = 200−250 K, whereas the corresponding temperature-dependent peculiarity in PL spectra is observed only for the lower energy PL peaks. The higher energy PL peaks instead follow the temperature dependence of uncoupled *J*-aggregates.

that all spectra originate from the very same hybrid system at different temperatures. We also note that no photodegradation of the sample was observed under the experimental conditions in the whole temperature range, allowing direct comparison between the different temperature-dependent PL spectra. The



DOI: 10.1021/acsphotonics.9b01079
ACS Photonics 2019, 6, 2570−2576

nanoparticle in this case was excited by a 532 nm laser. The inset displays the corresponding SEM image.

Probably the most interesting and peculiar spectroscopic features of the strongly coupled system are observed in the $T$ = 150−300 K range, while below $T$ = 150 K, the spectra are relatively temperature-independent. In particular, a substantial nonmonotonic red shift of both polaritonic branches in DF is observed at $T$ = 200−250 K, whereas upon further cooling, both peaks shift to the blue. This nonmonotonic temperature behavior correlates well only with the lower energy PL peak, whereas the higher energy PL peak does not follow this path. Instead, it follows the temperature behavior of the uncoupled *J*-aggregates (see Figure S1). Noteworthy, both uncoupled plasmons and uncoupled *J*-aggregates show relatively weak and monotonic temperature-dependent spectra (see Figure S1), which is in sharp contrast to the strongly coupled systems. These temperature-dependent measurements therefore allow to conclude that the lower energy PL peaks are indeed due to the lower polariton, in full agreement with the data recorded at fixed $T$ = 77 K in Figures 2−4. Correspondingly, the higher energy PL peak is not due to the upper polariton. Instead, the higher energy PL peak is due to emission from incoherent states and uncoupled molecules.

Additionally, it is noteworthy that the spectroscopic peculiarity, in all studied cases, seems to appear around the Debye temperature of silver ($T_\Theta \approx 221$ K, see Appendix for more details). Such temperature dependence is reproducible and further examples may be found in Figure S4. Noteworthy, no PL emission at the upper polariton frequency was observed in this study even at $T$ = 4 K. This is likely due to ultrafast relaxation into the dark states with a subsequent decay into the lower polariton.

The nonmonotonic temperature dependence of the lower polariton PL peak in Figure 5b can be understood using a polaron master equation approach.[39] By assuming that electronic excitations in individual aggregates are coupled to a harmonic oscillator bath with known spectral density $J(\omega)$, the lower polariton energy relative to the bare electronic resonance can be written as:

$$E_{\mathrm{LP}}(T) = -\sqrt{N}(\Omega_0/2)e^{-\Lambda(T)} - N\Omega_0^2 C(T)$$

where $\Omega_0$ is the bare Rabi frequency of an individual aggregate at zero temperature, and $N$ is the number of aggregates. The first term is the usual collective Rabi splitting ($\sqrt{N}$ scaling), modulated by a decreasing exponential factor with thermal exponent $\Lambda(T)$. The term that scales linearly with $N$ corresponds to the bath-induced collective Lamb shift. At low temperatures, both $\Lambda(T)$ and $C(T)$ scale as $a + bT^2$ with temperature ($a$ and $b$ being specific for $\Lambda$ and $C$). For $T \leq$ 100 K, both $\Lambda(T)$ and $C(T)$ are thus effectively temperature-independent, in agreement with Figure 5. Near $T \approx 150$ K, the Lamb shift term dominates the Rabi splitting due its stronger number scaling ($N$ vs $\sqrt{N}$). The lower polariton thus predominantly shifts to longer wavelengths with increasing temperature as $T^2$, up to a crossover temperature $T_c$. For temperatures beyond $T_c$, the lower polariton peak tends toward the bare electronic resonance. This occurs because the functions $C(T)$ and $e^{-\Lambda(T)}$ both decay rapidly with temperature in this regime. The open quantum system model that describes the results in Figure 5 is summarized in the Supporting Information, section S5. Further theoretical details will be provided elsewhere.[40]

## CONCLUSIONS

To conclude, we have performed a thorough correlative study between dark-field and photoluminescence spectroscopy of individual plasmon-molecule hybrid nanostructures in the strong coupling regime. The experiments were performed on individual silver nanoprisms surrounded by TDBC *J*-aggregates in a wide temperature range ($T$ = 4−300 K), under various laser excitations (532, 568, and 640 nm), and as a function of plasmon−exciton detuning. To ensure single particle performance, all optical data were accompanied by SEM imaging. To avoid any photodegradation of *J*-aggregates, all experiments were conducted using an optical cryostat.

Photoluminescence spectra for 532, 568, and 640 nm laser excitations show two, one, or no distinct emission peaks, correspondingly. In the case of 532 and 568 nm excitations, the lower energy PL peaks overlap with the corresponding LP DF peaks. Photoluminescence data from hybrids with blue and red plasmon-molecule detuning was studied. The presence of the lower polariton in PL is negligible in the blue-detuned cases, whereas in the red-detuned cases the lower polariton state is present, however, it appears broader and blue-shifted in comparison to the resonant case. Finally, temperature-dependent measurements show distinct red shifts in both polaritonic peaks occurring at $T$ = 200−250 K in dark-field spectra, which appear around the Debye temperature of silver ($T_\Theta \approx 221$ K). Such behavior can be explained by the polaron master equation approach. The corresponding PL spectra show the temperature-induced peculiarity only in the lower energy emission peak. The higher energy peak instead follows the temperature behavior of uncoupled molecules, which is almost temperature-independent. These experiments independently point toward lower polaritonic nature of the lower energy peak in PL, while the higher energy peak in PL is likely due to uncoupled molecules and incoherent states. These observations are in line with the previously reported theoretical models.[4−7,29,30]

Thus, our experimental findings improve the fundamental understanding of relaxation processes within plasmon−exciton hybrid systems. Since there has been a limited number of experimental studies on this matter,[8,26,27,31] it is important to further broaden the knowledge about the relaxation processes occurring in hybrid systems to facilitate development of future applications, such as stable nanoparticle hybrids[32] and room temperature single nanoparticle polaritonic lasers.

## METHODS

**Synthesis of Silver Nanoprisms.** In brief, a 3−5 nm silver seed nanoparticle solution was prepared by adding 1 mL of 30 mM trisodium citrate and 0.5 mL of 20 mM silver nitrate ($AgNO_3$) solutions to 95 mL of an ice-cold ultrapure distilled water. The solution was kept bubbling with $N_2$ under vigorous stirring in an ice-bath for an additional 60 min in the dark. Thereafter, 1 mL of ice-cold 50 mM $NaBH_4$ was added into the growth solution, at which point the color of the solution turns pale-yellow. Then 100 $\mu$L of 50 mM $NaBH_4$ was added subsequently to the solution. This procedure was repeated three more times with a 2 min break in between. The ice-cold and freshly prepared mixture of 1 mL of 5 mM bis(p-sulfonatophenyl)phenylphosphine dehydrate dipotassium salt (BSPP) and 1 mL of 50 mM $NaBH_4$ was added dropwise into the growth solution for seed nanoparticles. The solution was kept for 5 h in an ice bath under gentle stirring and completed



DOI: 10.1021/acsphotonics.9b01079
ACS Photonics 2019, 6, 2570−2576

with aging overnight in an ice bath under dark conditions. For the photoinduced growth of silver nanoparticles, 10 mL of the aged seed solution with pH = 9.5 was irradiated with a 532 nm continuous-wave (CW) laser. The reaction was allowed to proceed for 24 h, at which point the silver nanoparticles were washed two times by centrifugation at 3000 rcf for 5 min, whereupon the supernatant was removed and the remaining particles were redispersed in aqueous solution containing 0.3 mM of trisodium citrate.

**Synthesis of the Hybrid Nanostructures.** The hybrid nanostructures utilized in this study consist of self-assembled *J*-aggregates of TDBC dye molecules (5,6-dichloro-2- [[5,6-dichloro-1-ethyl-3-(4-sulfobutyl)-benzimidazol-2-ylidene]-propenyl]-1-ethyl-3-(4-sulfobutyl) benzimidazolium hydroxide, inner salt, sodium salt) on individual Ag nanoprisms, where the freshly synthesized Ag nanoparticles (1 mL) were finally embedded in molecular shells by mixing with 1 mL of the aqueous solution containing 0.1 mM TDBC dye molecules and 1 mM of KBr under gentle stirring for 15 min. The resulting colloidal solution was washed once by centrifugation (3000 rcf for 5 min). The supernatant was removed, and the remaining nanostructures were redispersed in distilled water and stored at 4 °C in the dark until use.

**Optical Spectroscopy.** The sample was prepared by drop casting 20 $\mu$L of hybrid nanoparticles solution on a polylysine-functionalized opaque $Si/SiO_2$ substrate. After 2 min, the solution was removed with a rapid extensive nitrogen flow. Exploiting a nanopatterned $Si/SiO_2$ substrate allows for spectroscopic and morphological correlation, as well as sufficient heat conductivity at cryogenic temperatures.

A bare *J*-aggregates sample was prepared from the solution containing 0.1 mM TDBC dye molecules and 1 mM of KBr with same procedure as for the hybrid nanoparticles. Dark-field scattering spectra were recorded using a reflective microscope (Nikon Y-IDP equipped with a 20×/NA = 0.4 bright-field objective) with a hyper-spectral imaging technique based on a liquid crystal tunable filter.[19] Both room temperature and cryogenic measurements were performed when the substrates were located inside a cryostat chamber (JANIS ST-500-UC), pumped to high vacuum ($\sim 10^{-5}$ Torr). The working distance of the dark-field scattering objectives, incorporated in the microscope, are too low to account for the distance between the lens and the substrate surface when the sample is places inside the cryostat chamber. Then, in order to mimic the dark-field scattering an external laser driven white-light source was utilized (Energetiq LDLS) at a high incident angle. In order to detect only the scattered light the sine of angle of the incident light needs to exceed the NA (~0.6) of the collecting objective.

For photoluminescence spectroscopy, we used a picosecond pulsed supercontinuum white-light laser (WhiteLase Micro, Fianuim) together with a suitable set of excitation, dichroic, and emission filters for 532, 568, and 640 nm excitations (all from Semrock). The photoluminescence experiments were conducted in the same optical cryostat and at the same temperatures as the corresponding dark-field measurements.

**Scanning Electron Microscopy.** Scanning electron microscopy (SEM) in a high-vacuum environment, with an acceleration voltage of 5 kV was utilized in order to image single silver nanoprisms. The prisms were located on top of an opaque silicon substrate with 55 nm $SiO_2$ layer on top, which ensured good enough electron conductivity to avoid any charging effects, which could cause distortion to the final image. The substrate was furthermore prepatterned from electron-beam lithography with different quadrants labeled *A*1, *A*2, ..., *A*15 to *O*1, *O*2, ..., *O*15, which enabled a straightforward navigation and, hence, also made it possible for a one-to-one correlation between optical scattering/PL data and SEM.

## ■ ASSOCIATED CONTENT

### Supporting Information

The Supporting Information is available free of charge on the ACS Publications website at DOI: 10.1021/acsphotonics.9b01079.

Additional information, control experiments, lifetime measurements, and additional modeling (PDF)

## ■ AUTHOR INFORMATION


### Corresponding Author

*E-mail: timurs@chalmers.se.

### ORCID

Denis G. Baranov: 0000-0002-8071-1587
Felipe Herrera: 0000-0001-8121-1931
Tomasz J. Antosiewicz: 0000-0003-2535-4174
Timur Shegai: 0000-0002-4266-3721


### Notes

The authors declare no competing financial interest.

## ■ ACKNOWLEDGMENTS

The authors acknowledge fruitful discussions with Dr. Betül Kücüköz and the financial support by the Swedish Research Council (Vetenskapsrådet) and the Engkvist Foundation.

## ■ REFERENCES


(1) Törmä, P.; Barnes, W. L. Strong coupling between surface plasmon polaritons and emitters: a review. *Rep. Prog. Phys.* **2015**, *78* (1), 013901.

(2) Baranov, D. G.; Wersall, M.; Cuadra, J.; Antosiewicz, T. J.; Shegai, T. Novel Nanostructures and Materials for Strong Light–Matter Interactions. *ACS Photonics* **2018**, *5*, 24.

(3) Tavis, M.; Cummings, F. W. The exact solution of N two level systems interacting with a single mode, quantized radiation field. *Phys. Lett. A* **1967**, *25*, 714–715.

(4) Agranovich, V. M.; Litinskaia, M.; Lidzey, D. G. Cavity polaritons in microcavities containing disordered organic semiconductors. *Phys. Rev. B: Condens. Matter Mater. Phys.* **2003**, *67* (8), 085311.

(5) Litinskaya, M.; Reineker, P.; Agranovich, V. M. Fast polariton relaxation in strongly coupled organic microcavities. *J. Lumin.* **2004**, *110* (4), 364–372.

(6) Litinskaya, M.; Reineker, P.; Agranovich, V. M. Exciton–polaritons in organic microcavities. *J. Lumin.* **2006**, *119–120*, 277–282.

(7) Herrera, F.; Spano, F. C. Dark Vibronic Polaritons and the Spectroscopy of Organic Microcavities. *Phys. Rev. Lett.* **2017**, *118*, na.

(8) Wersäll, M.; Cuadra, J.; Antosiewicz, T. J.; Balci, S.; Shegai, T. Observation of Mode Splitting in Photoluminescence of Individual Plasmonic Nanoparticles Strongly Coupled to Molecular Excitons. *Nano Lett.* **2017**, *17* (1), 551–558.

(9) Bellessa, J.; Bonnand, C.; Plenet, J. C.; Mugnier, J. Strong coupling between surface plasmons and excitons in an organic semiconductor. *Phys. Rev. Lett.* **2004**, *93* (3), 036404.

(10) Dintinger, J.; Klein, S.; Bustos, F.; Barnes, W. L.; Ebbesen, T. W. Strong coupling between surface plasmon-polaritons and organic molecules in subwavelength hole arrays. *Phys. Rev. B* **2005**, *71* (3), 035424.




DOI: 10.1021/acsphotonics.9b01079
*ACS Photonics* 2019, 6, 2570–2576

(11) Vasa, P.; Wang, W.; Pomraenke, R.; Lammers, M.; Maiuri, M.; Manzoni, C.; Cerullo, G.; Lienau, C. Real-time observation of ultrafast Rabi oscillations between excitons and plasmons in metal nanostructures with J-aggregates. *Nat. Photonics* **2013**, *7* (2), 128−132.
(12) Schwartz, T.; Hutchison, J. A.; Genet, C.; Ebbesen, T. W. Reversible Switching of Ultrastrong Light-Molecule Coupling. *Phys. Rev. Lett.* **2011**, *106* (19), 196405.
(13) Balci, S. Ultrastrong plasmon-exciton coupling in metal nanoprisms with J-aggregates. *Opt. Lett.* **2013**, *38* (21), 4498−4501.
(14) Väkeväinen, A. I.; Moerland, R. J.; Rekola, H. T.; Eskelinen, A.-P.; Martikainen, J.-P.; Kim, D.-H.; Törmä, P. Plasmonic Surface Lattice Resonances at the Strong Coupling Regime. *Nano Lett.* **2014**, *14* (4), 1721−1727.
(15) Ramezani, M.; Halpin, A.; Fernandez-Dominguez, A. I.; Feist, J.; Rodriguez, S. R.-K.; Garcia-Vidal, F. J.; Rivas, J. G. Plasmon-exciton-polariton lasing. *Optica* **2017**, *4*, 31−37.
(16) Schlather, A. E.; Large, N.; Urban, A. S.; Nordlander, P.; Halas, N. J. Near-Field Mediated Plexcitonic Coupling and Giant Rabi Splitting in Individual Metallic Dimers. *Nano Lett.* **2013**, *13* (7), 3281−3286.
(17) Zengin, G.; Johansson, G.; Johansson, P.; Antosiewicz, T. J.; Käll, M.; Shegai, T. Approaching the strong coupling limit in single plasmonic nanorods interacting with J-aggregates. *Sci. Rep.* **2013**, *3*, 3074.
(18) Itoh, T.; Yamamoto, Y. S.; Tamaru, H.; Biju, V.; Wakida, S.-i.; Ozaki, Y. Single-molecular surface-enhanced resonance Raman scattering as a quantitative probe of local electromagnetic field: The case of strong coupling between plasmonic and excitonic resonance. *Phys. Rev. B: Condens. Matter Mater. Phys.* **2014**, *89* (19), 195436.
(19) Zengin, G.; Wersäll, M.; Nilsson, S.; Antosiewicz, T. J.; Käll, M.; Shegai, T. Realizing strong light-matter interactions between single-nanoparticle plasmons and molecular excitons at ambient conditions. *Phys. Rev. Lett.* **2015**, *114* (15), 157401.
(20) Wen, J.; Wang, H.; Wang, W.; Deng, Z.; Zhuang, C.; Zhang, Y.; Liu, F.; She, J.; Chen, J.; Chen, H.; Deng, S.; Xu, N. Room-temperature vacuum Rabi splitting with active control in two-dimensional atomic crystals. *Nano Lett.* **2017**, *17*, 4689.
(21) Zheng, D.; Zhang, S.; Deng, Q.; Kang, M.; Nordlander, P.; Xu, H. Manipulating Coherent Plasmon-Exciton Interaction in a Single Silver Nanorod on Monolayer $WSe_2$. *Nano Lett.* **2017**, *17*, 3809.
(22) Kleemann, M.-E.; Chikkaraddy, R.; Alexeev, E. M.; Kos, D.; Carnegie, C.; Deacon, W.; de Pury, A. C.; Große, C.; de Nijs, B.; Mertens, J.; Tartakovskii, A. I.; Baumberg, J. J. Strong-coupling of $WSe_2$ in ultra-compact plasmonic nanocavities at room temperature. *Nat. Commun.* **2017**, *8* (1), 1296.
(23) Cuadra, J.; Baranov, D. G.; Wersäll, M.; Verre, R.; Antosiewicz, T. J.; Shegai, T. Observation of tunable charged exciton polaritons in hybrid monolayer $WS_2$-plasmonic nanoantenna system. *Nano Lett.* **2018**, *18*, 1777.
(24) Stührenberg, M.; Munkhbat, B.; Baranov, D. G.; Cuadra, J.; Yankovich, A. B.; Antosiewicz, T. J.; Olsson, E.; Shegai, T. Strong Light−Matter Coupling between Plasmons in Individual Gold Bi-pyramids and Excitons in Mono- and Multilayer $WSe_2$. *Nano Lett.* **2018**, *18* (9), 5938−5945.
(25) Santhosh, K.; Bitton, O.; Chuntonov, L.; Haran, G. Vacuum Rabi splitting in a plasmonic cavity at the single quantum emitter limit. *Nat. Commun.* **2016**, *7*, 11823.
(26) Groß, H.; Hamm, J. M.; Tufarelli, T.; Hess, O.; Hecht, B. Near-field strong coupling of single quantum dots. *Science Advances* **2018**, *4* (3), eaar4906.
(27) Leng, H.; Szychowski, B.; Daniel, M.-C.; Pelton, M. Strong coupling and induced transparency at room temperature with single quantum dots and gap plasmons. *Nat. Commun.* **2018**, *9* (1), 4012.
(28) Chikkaraddy, R.; de Nijs, B.; Benz, F.; Barrow, S. J.; Scherman, O. A.; Rosta, E.; Demetriadou, A.; Fox, P.; Hess, O.; Baumberg, J. J. Single-molecule strong coupling at room temperature in plasmonic nanocavities. *Nature* **2016**, *535* (7610), 127−130.
(29) del Pino, J.; Schröder, F. A. Y. N.; Chin, A. W.; Feist, J.; Garcia-Vidal, F. J. Tensor Network Simulation of Non-Markovian Dynamics in Organic Polaritons. *Phys. Rev. Lett.* **2018**, *121* (22), 227401.
(30) Neuman, T.; Aizpurua, J. Origin of the asymmetric light emission from molecular exciton-polaritons. *Optica* **2018**, *5* (10), 1247−1255.
(31) Melnikau, D.; Esteban, R.; Savateeva, D.; Sánchez-Iglesias, A.; Grzelczak, M.; Schmidt, M. K.; Liz-Marzán, L. M.; Aizpurua, J.; Rakovich, Y. P. Rabi Splitting in Photoluminescence Spectra of Hybrid Systems of Gold Nanorods and J-Aggregates. *J. Phys. Chem. Lett.* **2016**, *7* (2), 354−362.
(32) Munkhbat, B.; Wersäll, M.; Baranov, D. G.; Antosiewicz, T. J.; Shegai, T. Suppression of photo-oxidation of organic chromophores by strong coupling to plasmonic nanoantennas. *Science Advances* **2018**, *4* (7), eaas9552.
(33) Coles, D. M.; Meijer, A. J. H. M.; Tsoi, W. C.; Charlton, M. D. B.; Kim, J.-S.; Lidzey, D. G. A Characterization of the Raman Modes in a J-Aggregate-Forming Dye: A Comparison between Theory and Experiment. *J. Phys. Chem. A* **2010**, *114* (44), 11920−11927.
(34) Peters, V. N.; Faruk, M. O.; Asane, J.; Alexander, R.; Peters, D. a. A.; Prayakarao, S.; Rout, S.; Noginov, M. A. Effect of strong coupling on photodegradation of the semiconducting polymer P3HT. *Optica* **2019**, *6* (3), 318−325.
(35) Michetti, P.; La Rocca, G. C. Polariton states in disordered organic microcavities. *Phys. Rev. B: Condens. Matter Mater. Phys.* **2005**, *71* (11), 115320.
(36) Michetti, P.; La Rocca, G. C. Simulation of J-aggregate microcavity photoluminescence. *Phys. Rev. B: Condens. Matter Mater. Phys.* **2008**, *77* (19), 195301.
(37) Coles, D. M.; Michetti, P.; Clark, C.; Tsoi, W. C.; Adawi, A. M.; Kim, J.-S.; Lidzey, D. G. Vibrationally Assisted Polariton-Relaxation Processes in Strongly Coupled Organic-Semiconductor Microcavities. *Adv. Funct. Mater.* **2011**, *21* (19), 3691−3696.
(38) Rudin, S.; Reinecke, T. L.; Segall, B. Temperature-dependent exciton linewidths in semiconductors. *Phys. Rev. B: Condens. Matter Mater. Phys.* **1990**, *42* (17), 11218−11231.
(39) Xu, D.; Cao, J. Non-canonical distribution and non-equilibrium transport beyond weak system-bath coupling regime: A polaron transformation approach. *Frontiers of Physics* **2016**, *11* (4), 110308.
(40) Herrera, F.; Wersäll, M.; Shegai, T.; Cao, J. Manuscript in preparation, 2019.



DOI: 10.1021/acsphotonics.9b01079
*ACS Photonics* 2019, 6, 2570−2576